Nuclear Engineering and Technology 55 (2023) 2941–2951

Contents lists available at ScienceDirect

Nuclear Engineering and Technology

journal homepage: www.elsevier.com/locate/net

Original Article

Evaluation of ECCD power requirement for neoclassical tearing modes suppression in the CFETR hybrid scenario

L.H. He [a], P.W. Zheng [a, b, *], T. Yu [a, **]

[a] School of Nuclear Science and Technology, University of South China, Hengyang, Hunan Province, 421001, PR China
[b] School of Resource Environment and Safety Engineering, University of South China, Hengyang, Hunan Province, 421001, PR China

ARTICLE INFO

Article history:
Received 17 October 2022
Received in revised form
30 March 2023
Accepted 29 April 2023
Available online 5 May 2023

Keywords:
CFETR
Electron cyclotron current drive (ECCD)
Neoclassical tearing mode (NTM)
Modified Rutherford equation (MRE)
3/2 mode
2/1 mode

ABSTRACT

The optimal minimum ECCD power is evaluated numerically for completely suppressing the 3/2 and 2/1 NTMs in the CFETR hybrid scenario. For two typical frequencies of ECCD sources launching from two upper launcher (UL) ports, $f_{ec} = 210$ GHz and 240 GHz with O1-mode, UL_1: $(R_i, Z_i) = (8.47, 5.7)$ m and UL_2: $(R_i, Z_i) = (8.2, 4.5)$ m, higher frequency of ECCD source launching from the UL_2 port is better than that low frequency counterpart from the UL_1 port. Using 240 GHz ECCD source launching from the UL_2 port, the minimum power required to fully suppress the two NTMs with precise ECCD alignment is 12.4 MW and 16.7 MW, respectively. When good alignment cannot be achieved, the results suggest that the misalignment should not exceed $0.02a$, preferably $0.015a$, corresponding to 4.4 cm and 3.3 cm. Considering engineering difficulty of high-frequency gyrotron sources, the optimal minimum ECCD power with the 210 GHz source launching from the UL_2 port is 17.9 MW and 20.6 MW for completely suppressing the 3/2 and 2/1 NTMs, respectively. In view of this, it is a good choice to select the 210 GHz ECCD source launching from the UL_2 port in the short and medium term.
© 2023 Korean Nuclear Society, Published by Elsevier Korea LLC. This is an open access article under the CC BY-NC-ND license (http://creativecommons.org/licenses/by-nc-nd/4.0/).

1. Introduction

The China Fusion Engineering Test Reactor (CFETR) [1–3] will bridge the gap between the International Thermonuclear Experimental Reactor (ITER) and the fusion demonstration reactor (DEMO) to demonstrate related technologies and physics models. The concept and engineering designs of the CFETR were completed in 2020 [3], the main parameters of the CFETR are $R = 7.2$ m, $a = 2.2$ m, $B_T = 6.5$ T [3,4]. These main parameters are now solidified and used to guide physics design activities. The CFETR will demonstrate the feasibility of continuous large scale fusion energy for stable and safe power generation over 1 GW.

The electron cyclotron (EC) system in ITER has the highest flexibility by combining the equatorial launcher (EL) and the upper launcher (UL), the EC power deposition can cover up to 85% of the plasma cross-section, allowing for central heating, current profile tailoring and magneto-hydrodynamics (MHD) stability control of such as neoclassical tearing modes (NTMs) in the flat-top phase of the plasma [5]. The EC system is also one of main external heating and current drive systems planned in CFETR. Given the ratio of toroidal magnetic fields in ITER and CFETR, one might expect that a EC frequency of around 210 GHz would be suitable for CFETR. W. Wei et al. found that the highest current drive efficiency can be obtained at this frequency with the toroidal field of 6.5 T. The efficiency of electron cyclotron current drive (ECCD) gradually increases with the increase of frequency [6,7]. However, the fraction of higher harmonic absorption also increases rapidly for EL manner [8], and EL-ECCD always has a wider profile which is detrimental to the suppression of NTMs. An important application of the EC systems is NTMs suppression especially for $m = 3/n = 2$ (3/2) and $m = 2/n = 1$ (2/1) modes, where m and n are the poloidal and toroidal mode number, respectively. The UL manner has been drawn special attention as it can provide localized deposition down to 2% of the minor radius [5], and avoid the detrimental higher harmonic absorption of EC power in the edge region [8]. Depositing EC power inside a magnetic island, localized ECCD is an effective method for suppressing of 3/2 and 2/1 NTMs by driving localized current profile at the rational surface $q = 1.5$ and $q = 2$ [9].

Evaluation of the EC power needed for NTMs stabilization in the ITER baseline are usually expressed in terms of the figure of merit $\eta_{NTM} \equiv j_{CD}/j_{BS}$, the ratio of the EC driven current density to the

* Corresponding author. School of Nuclear Science and Technology, University of South China, Hengyang, Hunan Province, 421001, PR China.
** Corresponding author.
E-mail addresses: pwzheng@usc.edu.cn (P.W. Zheng), yutao29@sina.com (T. Yu).

https://doi.org/10.1016/j.net.2023.04.046
1738-5733/© 2023 Korean Nuclear Society, Published by Elsevier Korea LLC. This is an open access article under the CC BY-NC-ND license (http://creativecommons.org/licenses/by-nc-nd/4.0/).

bootstrap current density at the rational surface. Followed the work of Hegna and Callen [10] who predicted $\eta_{NTM} = 1.5$ for ITER, Zohm [11] predicted $\eta_{NTM} = 1.2$. The figure of merit $\eta_{NTM} = 1.2$ is also used to assess the performance of the electron cyclotron wave system in HL-2M tokamak [12]. However, the figure of merit $\eta_{NTM} = 1.2$ may can't be applied directly for the CFETR configuration to assess the power needed for NTMs control, because the size and the toroidal magnetic field of the CFETR tokamak is larger than that of the ITER. In addition, the ECCD efficiency at the target rational surface is dependent on kinetic profiles (electron density n_e and temperature T_e), launcher position and incident angles, and the ratio of magnetic field strength to EC source frequency. Hence, it is necessary to couple a ray-tracing code with a modified Rutherford equation (MRE) to evaluate the minimum EC power needed for 3/2 and 2/1 NTMs control on CFETR scenarios. Although lower hybrid wave can drive localized non-inductive currents in DEMO, the driven currents have only major peaks near the edge of plasma [13] and cannot be used to suppress NTMs.

As the developed CFETR steady-state scenario by integrated modeling has no $q = 1.5$ and $q = 2$ rational surfaces [3], in this paper assessment of EC power requirement for 3/2 and 2/1 NTMs stabilization is studied under CFETR hybrid scenario. In section 2, the coupled ray-tracing model and MRE are introduced, this method is used to the studies of this paper. Section 3 presents detail the results and discussion. Finally, section 4 summarizes and concludes the paper.

2. Method

More precisely, NTM suppression needs to be simulated self-consistently with integrated modelling incorporating equilibrium, current diffusion, heating and current drive, and island evolution [14–17]. However, the total driven current of ECCD used to suppress NTM is generally much smaller than the plasma current. Although ECCD can change the magnetic equilibrium and thus affect its power deposition position, the magnitude of the effect causing the ECCD position to move should be small and can be taken into account in the misalignment effect. Moreover, on CFETR devices, the magnitude of the toroidal magnetic field, $B_T = 6.5$ T, is much higher than the magnetic field of current tokamak devices. Therefore, the magnetic field perturbation generated by ECCD is much smaller than B_T, and the impact of ECCD itself on the magnetic equilibrium that evolves over time will also be small. Hence, this work assumes that changes in equilibrium and the effect of current diffusion are not considered while ECCD is applied.

In order to assess the EC system requirements for the CFETR, it is important to obtain the ECCD information at target rational surface under specific operation scenario, the information can be calculated by a ray-tracing method, such as the GENRAY [18] code. After that, the peak EC current density j_{ec}, full width w_{dep} (1/e) of driven current profile and misalignment of target rational surface $\Delta\rho = |\rho_{rs} - \rho_{ec}| = |\rho_{m/n} - \rho_{ec}|$ are then coupled to the MRE to calculate the minimum EC power for stabilizing the 3/2 and the 2/1 NTMs.

2.1. Ray-tracing method for calculation of ECCD

The trajectories of EC waves and associated driven current are calculated by the GENRAY code. The dispersion relation of cold plasma is used to simulate the EC propagation in tokamak plasma, the Mazzucato relativistic model [19] is used to compute the EC power absorption, and the Lin-Liu model [20] for current drive efficiency with parallel momentum conservation [21,22] of electron-electron collision operator is used to calculate ECCD in general geometry. Hence, the obtaining of the ECCD profile does not need to couple ray-tracing with the Fokker-Planck method [23].

GENRAY code determines the ray trajectories from the following system of the ordinary differential equation:

$$\frac{d\boldsymbol{X}}{dt} = -\frac{\partial D/\partial \boldsymbol{k}}{\partial D/\partial \omega}, \tag{1}$$

$$\frac{d\boldsymbol{k}}{dt} = \frac{\partial D/\partial \boldsymbol{X}}{\partial D/\partial \omega}, \tag{2}$$

where $\omega = 2\pi f_{ec}$ is angular frequency of EC waves, $\boldsymbol{X}$ is the spatial position vector, $\boldsymbol{k}$ is the wave vector, and D is the real part determined from the cold plasma dispersion relation. The wave power P along the ray trajectory can be found in the following equation,

$$P(s) = P_{in}\exp\left(-2\int_0^s \mathrm{Im}(\boldsymbol{k})\bullet d\boldsymbol{s}\right). \tag{3}$$

The imaginary part of $\boldsymbol{k}$ is obtained from solving the dispersion relation. $\boldsymbol{s}$ is the vector directed parallel the trajectory, s is the distance along the ray trajectory, P_{in} is the wave power at launch point. The integral is calculated along the ray trajectory. The Lin-Liu model is used to calculate the current drive efficiency j/P by the adjoint approach [20,24]. Different ray/beam-tracing linear codes and Fokker-Planck quasilinear solvers have been benchmarked thoroughly for ECCD in ITER scenarios [25]. In GENRAY code, the incident angles (α, β) are used to change the radial location of ECCD in CFETR, where the toroidal incident angle α refers to the angle measured counterclockwise along the major radius on the equatorial plane at the launching position, and the poloidal incident angle β refers to the angle measured from the vertical direction counterclockwisely.

2.2. The modified Rutherford equation (MRE)

The contributions from the ECCD added to the MRE using the formulae by Bertelli et al. [26] and De Lazzari et al. [27]. Retaining the most relevant terms, the MRE is written as following [26,27],

$$0.82\frac{\tau_r}{r_s}\frac{dw}{dt} = r_s\Delta_0' + r_s\delta\Delta_0' + r_s\Delta_{BS}' + r_s\Delta_{CD}', \tag{4}$$

where $\tau_r \equiv \mu_0 r_s^2/\eta$ is the local resistive time for the resistivity η at the rational surface r_s of the interested NTM, and μ_0 is the permeability of free space. The terms on right hand side provide the effect of the linear stability index Δ_0', the variation of Δ_0' due to the perturbation of the equilibrium current $\delta\Delta_0'$, the perturbation of the bootstrap current Δ_{BS}', and the perturbation of localized non-inductive current drive by electron cyclotron waves Δ_{CD}', respectively. Details of the right-hand-side terms of the MRE for the evolution of the island width are summarized in the Appendix A In addition, this paper assumes perfect alignment of ECCD to the island O-point.

2.3. Coupling method and simulation scenario

The ECCD characteristic quantities ρ_{ec}, j_{ec} (unit: A·cm^{-2}MW^{-1}) and w_{dep} that calculated by the GENRAY code are used to construct a Gaussian current profile according to the equation

$$j_{CD} = j_{ec}\exp\left(-(\rho-\rho_{ec})^2 \Big/ \left(\left(\frac{w_{dep}}{2}\right)^2\right)\right) \tag{5}$$

These characteristic quantities are passed to the MRE to calculate the growth rate of a NTM magnetic island width with time if the Gaussian fitted profile by equation (5) is in good agreement

with that of the GENRAY calculation. In fact, this condition can be satisfied in most cases, even if the ECCD profile calculated by GENRAY is not smooth, it can be made to conform to the Gaussian distribution by smoothing the curve. Fig. 1 shows the examples of fitting GENRAY results with the Gaussian form based on equation (5). For the best fitting case, Fig. 1 (a), the original curve obtained by GENRAY code, the smoothed curve and the Gaussian fitted curve are almost identical. For the worst fitting case, Fig. 1 (b), the ECCD profile calculated by GENRAY has some burrs, the characteristic quantities of ECCD are extracted from the smoothed curve to form a Gaussian profile. As shown in Fig. 1, the Gaussian fitted curve has a lower value of peak current density compared to the original one, it will increase the calculated EC power demand required to suppress NTMs, and the resulting results will be somewhat conservative.

Due to large volume of the CFETR device, the EC power density P_{EC} in the plasma is well below the limit of non-linear effect [7]: $P_{EC}[MW\cdot m^{-3}]/(n_e[10^{19}m^{-3}])^2 \geq 0.5$ [28]. Hence, the current drive efficiency is independent on EC power for specific EC launching condition, the ECCD is scaled linearly with the absorbed EC power P_{abs}. In the cases of full absorption, it is scaled linearly with the input EC power P_{in}. Combining with the MRE, the minimum EC power for fully suppressing NTMs can be obtained.

For the simulation CFETR scenarios, as described in the introduction section, only the hybrid operation scenario [3,4] is considered, the plasma current I_p = 13 MA. The magnetic flux surfaces of the CFETR hybrid scenario are shown in Fig. 2. The corresponding kinetic profiles and profiles of bootstrap current density j_{BS} and safety factor q are shown in Fig. 3. The profile of q monotonically increases as the normalized radial position ρ, it is not necessary to consider ECCD control of TMs/NTMs with reversed magnetic shear tokamak plasmas [29,30]. The radial positions of q = 1.5 and q = 2 rational surfaces are $\rho_{3/2}$ = 0.4321 and $\rho_{2/1}$ = 0.5576, respective. Although some hybrid scenarios found on DIII-D, these scenarios rely on poloidal magnetic-flux pumping by 3/2 TM to maintain the q-profile [31,32], in this paper the flux pumping effect is not considered in the investigation of 3/2 NTM suppression in the CFETR hybrid scenario.

For the EC launcher position and frequency, according to the results of references [4,6,7] and analysis in introduction, two EC waves with different frequencies launching from two different upper launcher ports are considered in the simulations. One frequency of EC wave is f_{ec} = 210 GHz, another is f_{ec} = 240 GHz, the two frequencies are fundamental ordinary mode (O1-mode). As shown in Fig. 2, two upper launcher ports are used to launching EC waves: UL_1, (R_i, Z_i) = (8.47, 5.7) m [6], and UL_2, (R_i, Z_i) = (8.2, 4.5) m [4,7]. The f_{ec} = 240 GHz of O1-mode is chosen as this frequency is the best candidate for efficient and flexible ECCD under the CFETR parameters [7] despite of the greater engineering manufacturing difficulty. As a result, a total of four ECCD cases listed in Table 1 are

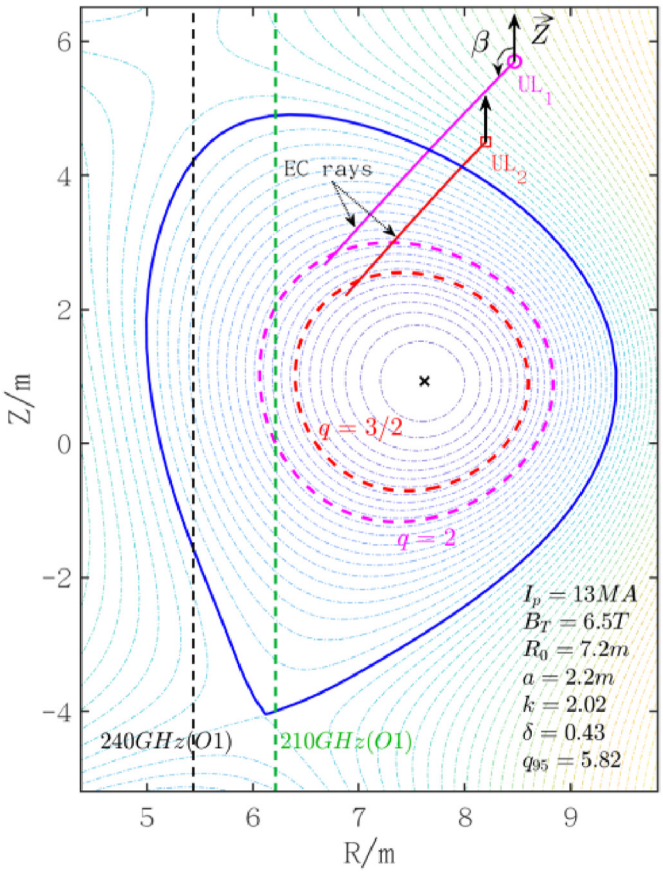

Fig. 2. CFETR hybrid scenario with I_p = 13.0 MA and B_T = 6.5 T. The two dashed contours are the flux surfaces of q = 2, q = 3/2. The magenta circle and red square indicate the locations of the two upper launchers (UL_1, R = 8.47 m, Z = 5.7 m) and (UL_2, R = 8.2 m, Z = 4.5 m), respectively. The poloidal injection angle β and the resonance curves are marked in the panel. (For interpretation of the references to colour in this figure legend, the reader is referred to the Web version of this article.)

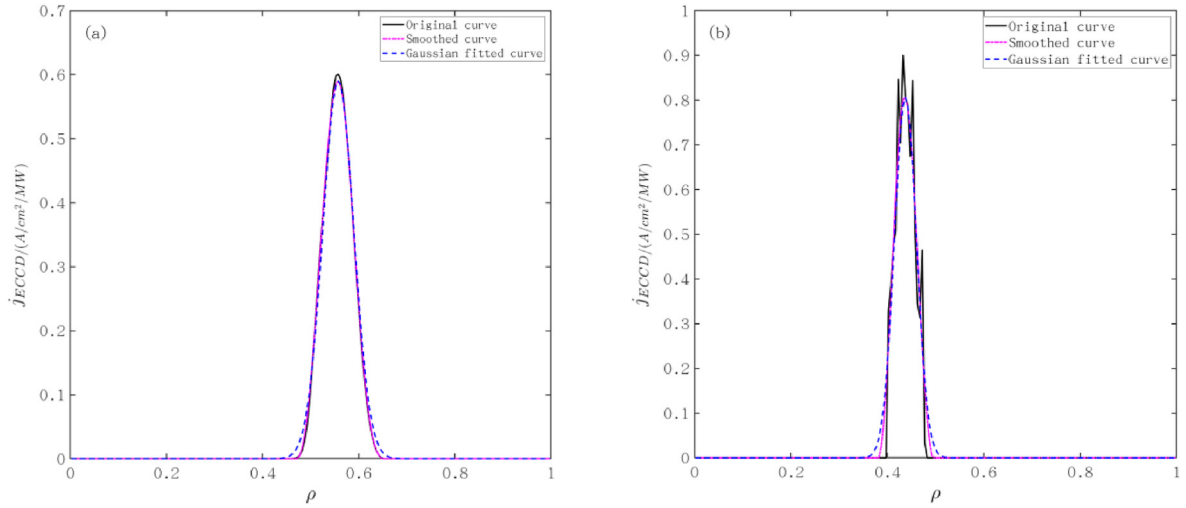

Fig. 1. Examples of fitting GENRAY results with the Gaussian form. (a) the best fitting case, and (b) the worst fitting case. The original curves are calculated by GENRAY under the CFETR hybrid scenario with EC frequency of 210 GHz.

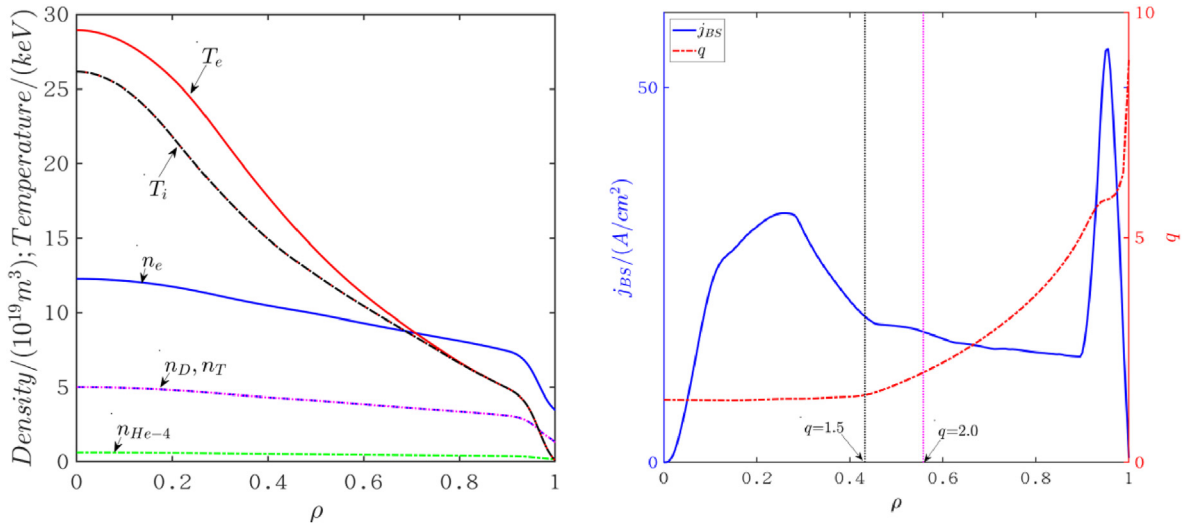

Fig. 3. Kinetic profiles and profiles bootstrap current density j_{BS} and safety factor q of CFETR hybrid scenario. The radial positions of $q = 1.5$ and $q = 2$ rational surfaces are shown in the right plot.

used to drive the local currents on the 3/2 and 2/1 magnetic surfaces according to the permutation. For each case, the optimum minimized EC power needed for completely stabilizing the two NTMs are determined by changing the incident angles (α, β).

The necessary physical quantities used in the MRE (4) are listed in Table 2. Letting the value of misalignment $\Delta\rho = |\rho_{ec} - \rho_{rs}| = |\rho_{ec} - \rho_{m/n}|$ approaching zero as close as possible, the GENRAY code is used to calculate the characteristic physical quantities of ECCD, the j_{ec}, w_{dep} and I_{ec} etc. This is achieved by changing the poloidal injection angle β under a given toroidal injection angle α.

3. Results and discussion

3.1. Results of NTMs suppression by EC wave with $f_{ec} = 210$ GHz

For the cases A and B, the EC wave with EC frequency $f_{ec} = 210$ GHz is launched from the UL_1 and UL_2 ports, respectively. The results of ECCD near the $q = 1.5$ and $q = 2$ rational surfaces are shown in Fig. 4, and the dependence of minimum EC power P_{min} for suppressing the 3/2 and 2/1 NTMs on toroidal injection angle α is shown in Fig. 5.

As shown in Fig. 4, with the value of α increases from 192° to 230° at 2° intervals, the values of w_{dep} and I_{ec} increases for ECCD near the 3/2 and 2/1 rational surfaces, but the value of j_{ec} decreases only for ECCD near the 3/2 rational surface. However, for ECCD near the 2/1 rational surface the value of j_{ec} increases first then drops with the increase of α. Compared with launching port from UL_1, the UL_2 port makes ECCD have larger values of j_{ec} and I_{ec} and smaller value of w_{dep}/a. Although a large toroidal incident angle (220° ~ 230°) is used for numerical simulation in this paper, its feasibility needs to be considered in engineering. This can be achieved through the design of launching mirrors of EC systems.

Perfect alignment is a critical factor for effective NTM suppression by ECCD. Except $\alpha = 192°$, misalignment $\Delta\rho = |\rho_{rs} - \rho_{ec}| = |\rho_{3/2} - \rho_{ec}| = 0.0054$, the $\Delta\rho$ equals to 0.0004 for ECCD near the 3/2 rational surface; and the $\Delta\rho$ equals to 0.0001 for ECCD near the 2/1 rational surface. Thus, the positions of these ECCD are well aligned with the 3/2 and the 2/1 rational surfaces.

Table 1
Simulation cases of ECCD to drive localized current at target 3/2 and 2/1 magnetic surfaces.

Case	f_{ec}/(GHZ)	UL port
A	210	UL_1: $(R_i, Z_i) = (8.47, 5.7)$ m
B	210	UL_2: $(R_i, Z_i) = (8.20, 4.5)$ m
C	240	UL_1: $(R_i, Z_i) = (8.47, 5.7)$ m
D	240	UL_2: $(R_i, Z_i) = (8.20, 4.5)$ m

From Fig. 4 (c) and (f), more efficient current drive needs a larger value of α, but this results in a wider driven current profile (Fig. 4 (b) and (e)). While too larger of a value of w_{dep} is usually bad for NTM stabilization. Due to the typical value of w_{dep} is 0.1–0.2 which represents a wider ECCD profile, modulate ECCD is more efficient for a NTM suppression than continue manner. In this paper, the duty cycle D_m of modulated ECCD is set to 0.5 when calculating the EC power using MRE. In addition, a more peaked ECCD is more conducive to suppressing NTM. For different toroidal injection angles, there must be an optimal value of α_{opt} such that the minimum EC power P_{min} required to fully suppress a NTM reaches a certain minimum value.

Fig. 5 shows the minimum EC power P_{min} for 3/2 and 2/1 NTMs decrease first with the increase of toroidal injection angle α then increase. For UL_1 port, the minimum values of P_{min} for the 3/2 and 2/1 NTMs are 25.8 MW and 26.0 MW, respectively. The corresponding optimum incident angles are (α, β) = (204°, 150.0°) and (208°, 145.0°). For UL_2 port, the corresponding minimum values P_{min} of are 17.9 MW and 20.6 MW, and the optimum incident angles are (α, β) = (214°,143.1°) and (218°,137.3°).

As shown in Fig. 4, although the value of j_{ec} at 2/1 rational surface is smaller than that at the 3/2 rational surface, the value of w_{dep}/a at 2/1 rational surface is also smaller for most value of α. The result is that the minimum EC power P_{min} required to fully suppress 3/2 NTM is not significantly lower than that of the 2/1 NTM, despite the higher efficiency of the ECCD at the 3/2 rational surface. Especially at larger α values for UL_1 launching case which is shown in Fig. 5 (a), the minimum EC power required to completely suppress the 2/1 NTM is surprisingly smaller compared that of the 3/2 NTM. Even for UL_2 launching case, Fig. 5 (b) shows that the minimum EC power for completely suppressing the 3/2 and the 2/1 NTMs are very close at large value of α ($\alpha \geq 220°$). The reason is that when the value of α is large, as shown in Fig. 4 (a)–(b) and (d) - (e), the width w_{dep}/a of the driven current of ECCD on the 3/2 rational surface is much larger which is usually bad to the stability of NTM, while the value difference between $j_{ec,3/2}$ and $j_{ec,2/1}$ is not significant.

However, it should be pointed out that the equilibrium evolution due to ECCD and current diffusion, the island position evolves according to the equilibrium. In this case, a slightly broader

Table 2
Physical quantities used in MRE at 3/2 and 2/1 rational surfaces.

Physical quantities	3/2 mode	2/1 mode
Normalized radial location of rational surface $\rho_{m/n} = r_{m/n}/a$	0.4321	0.5576
Local electron density $n_e/(10^{19}m^{-3})$	10.28	9.55
Local electron temperature T_e/(keV)	16.55	12.40
Local magnetic shear length $L_q = q/(dq/dr)$/(cm)	163.68	88.49
Local bootstrap current density $j_{BS}/(A/cm^2)$	19.49	17.41
Local inverse aspect ratio $\varepsilon = r_{rs}/R$	0.132	0.170
Local poloidal magnetic field strength B_{th}/(T)	0.656	0.635

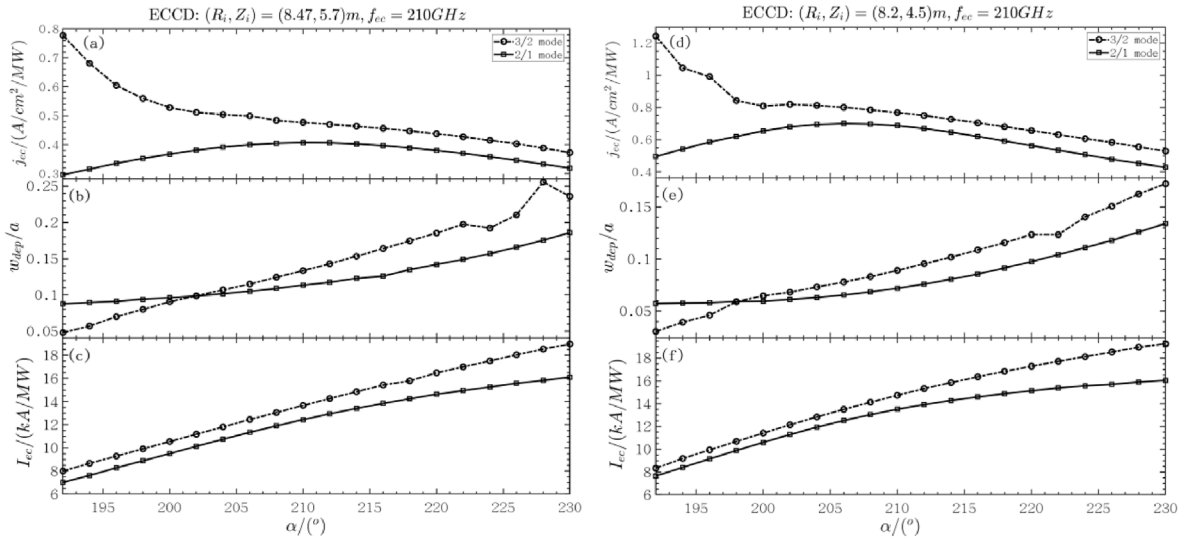

Fig. 4. Results of ECCD near the $q = 1.5$ and $q = 2$ rational surface under different α for cases A and B. (a)–(c): Case A, EC wave is launched from UL_1 port. (d)–(f): Case B, EC wave is launched from UL_2 port. EC frequency $f_{ec} = 210$ GHz.

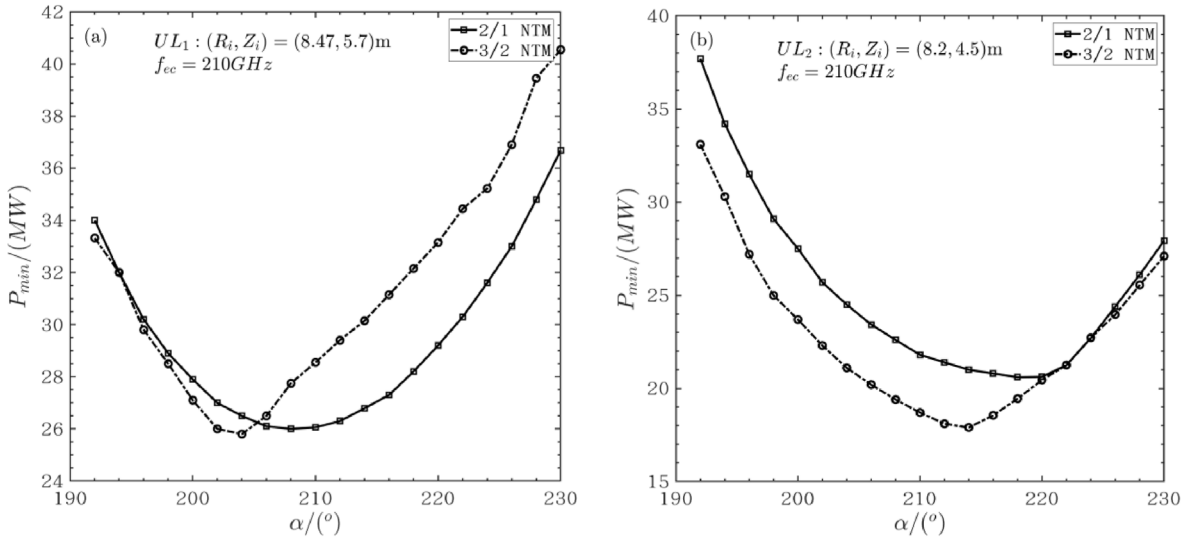

Fig. 5. The dependence of minimum EC power P_{min} on toroidal injection angle α for cases A and B. (a) Results of case A. (b) Results of case B. EC frequency $f_{ec} = 210$ GHz.

deposition width is more desirable since the narrow deposition could destabilize the island easily due to misalignment with the island [33].

Fig. 6 (a) shows the relationship between the growth rate of 2/1 NTM magnetic island and the width of magnetic island with and without UL_2-ECCD (f_{ec} = 210 GHz). The minimum EC power requirement for fully stabilization of the 2/1 NTM is found to be $P_{min} = 20.6$ MW, at which power level the $dw/dt < 0$ for all magnetic island width w. This makes the figure of merit η_{NTM} for completely stabilizing of the 2/1 NTM equal to 0.7. Here $\eta_{NTM} \equiv j_{CD,max}/j_{BS} = j_{ec} \cdot P_{min}/j_{BS}$. The total driven current I_{tot} only accounts for 2.36% of the plasma current I_p: $(I_{tot}/I_p) \times 100\% = (I_{ec} \cdot P_{min}/I_p) \times 100\% = 2.36\%$. Fig. 6 (b) show the corresponding driven current profile of the optimum UL_2-ECCD with 210 GHz, and how the characteristic physical quantities (j_{ec}, $\Delta\rho$, ρ_{ec}, w_{dep}/a, etc.) which need by MRE are obtained from the ECCD profile.

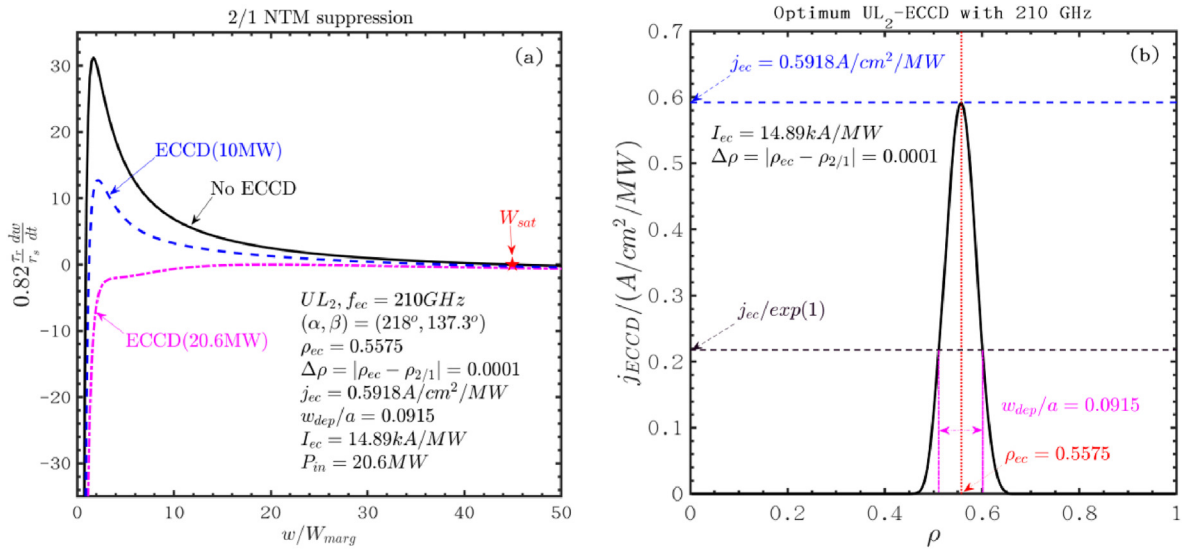

Fig. 6. (a) Growth rate of the 2/1 NTM versus the island width. (b) The corresponding driven current profile and characteristic physical quantities of the optimum UL_2-ECCD with 210 GHz.

3.2. Results of NTMs suppression by EC wave with $f_{ec} = 240$ GHz

The results in section 3.2 show that when the frequency of EC is 210 GHz, the range of the toroidal incident angle α that makes the ECCD well aligned with the 3/2 and 2/1 rational surfaces is relatively large, from 192° to 230°, and the upper launcher position of EC wave has little effect. When other conditions remain unchanged but the frequency of EC wave increases to 240 GHz, the range of the value of α becomes smaller. Similarly, the upper launcher position has little effect. As shown in Fig. 7, the range of the value of α is [216°, 230°] for 3/2 NTM, and [206°, 230°] for 2/1 NTM. For the value of α less than the minimum value in these two ranges, the ECCD cannot be well aligned with the rational surfaces by adjusting the poloidal injection angle β.

For the ECCD results with EC frequency $f_{ec} = 240$ GHz, the trend of j_{ec}, w_{dep}/a and I_{ec} with the toroidal injection angle α is the same as that in Fig. 4. However, compared to the results of ECCD with frequency $f_{ec} = 210$ GHz, the peak value (j_{ec}) and the current value driven by unit power (I_{ec}) are larger, but the width of driven ECCD (w_{dep}/a) is smaller. These are better for complete suppressing of the 3/2 and 2/1 NTMs. It means that the optimum minimum EC power needed for complete suppressing these NTMs will be smaller. Fig. 8 shows the results of the dependence of minimum EC power P_{min} on toroidal injection angle α for cases C and D. It is obvious that under the condition of the same value of α, the higher frequency (240 GHz) of EC wave requires less power for completely suppressing NTMs. Similarly, for UL_1 port, the minimum values of P_{min} for the 3/2 and 2/1 NTMs are 13.4 MW and 17.3 MW, respectively. The corresponding optimum incident angles are (α, β) = (220°, 143.0°) and (216°, 139.2°). For UL_2 port, the corresponding minimum values P_{min} of are 12.4 MW and 16.7 MW, and the optimum incident angles are (α, β) = (222°,136.6°) and (216°,130.4°).

In order to compare the influence of the upper launcher position and frequency of EC wave under optimal conditions, we summarize the optimum minimum EC power for the four cases, the case A - D. The results are presented in Table 3 together with the injection angles to obtain these results. We find that both the upper launcher position and EC frequency have a great impact on NTMs suppression. UL_2 is better than UL_1, the decrease of optimal P_{min} is obvious for low-frequency EC wave ($f_{ec} = 210$ GHz), but not obvious for high-frequency EC wave ($f_{ec} = 240$ GHz). However, when the wave frequency is increased from 210 GHz to 240 GHz, the reduction magnitude of optimal P_{min} is significant and larger. It should be noted that EC wave with higher frequency, such as $f_{ec} = 240$ GHz used in this paper for the purpose of numerical investigation, is more difficult to develop. For CFETR device operating in a 6–7 T toroidal magnetic field, it is expected that the long pulse gyrotron with a frequency of 210 GHz will be easier and faster to develop in engineering than 240 GHz.

Some other factors affecting NTMs stabilization are not considered in this paper, such as: (1) the influence of magnetic island on EC wave propagation, power deposition and current drive [34], (2) the ECCD profile in reality is the superposition of multiple individual EC beams from distinct wave-guides, (3) the influence of electron density fluctuation on the reduction of current drive efficiency and widening of driven current profile [35], and (4) the Reiman-Fisch current condensation effect [36]. For the factor (1), due to large value of toroidal magnetic field of CFETR, $B_T = 6.5$ T, and such a high frequency of a EC beam, $f_{ec} \geq$ ~ 210 GHz, the influence of this factor on NTM suppression can be ignored. The effect of the superposition of individual EC beams may slightly widening the driven ECCD profile, this may result in a slight increase in the required EC wave power. Although the density fluctuation effect will cause the ECCD to be broadened, resulting in an increase in the required EC wave power, it still needs to be experimentally verified on the reactor level tokamak device, such as ITER device. As for the Reiman-Fisch current condensation effect, due to the large size of the CFETR device, $R = 7.2$ m, $a = 2.2$ m, and relatively larger value (~0.1) of w_{dep}/a for the ECCD in CFETR plasma, the effect should be small.

At the end of this section, we also summarize the value of η_{NTM} and $(I_{tot}/I_p) \times 100\%$ under the optimum conditions. The results are shown in Table 4. The maximum value of η_{NTM} will not more than 1.0 under the optimum conditions. And the total driven current I_{tot} is still very small compared with the plasma current ($I_p = 13$ MA), and the ratio of the two is not more than 2.4%.

3.3. Effect of misalignment on the stabilization

The effect of misalignment between the ECCD location and the rational surfaces where the NTMs are triggered has been studied [27,35–39]. It is concluded that the keeping alignment within $0.5w_{dep}$ is a necessary requirement. Similarly, we found that misalignment has a significant impact on 2/1 and 3/2 NTMs stabilizing by ECCD in the CFETR configuration. In addition, UL position

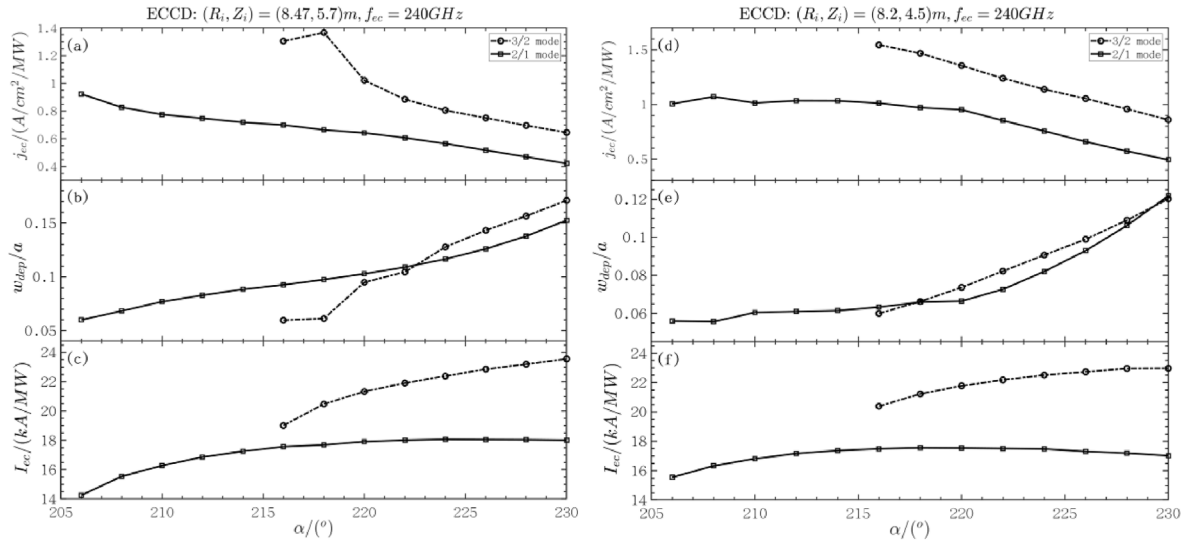

Fig. 7. Results of ECCD near the $q = 1.5$ and $q = 2$ rational surface under different α for cases C and D. (a)–(c): Case C, EC wave is launched from UL_1 port. (d)–(f): Case D, EC wave is launched from UL_2 port. EC frequency $f_{ec} = 240$ GHz.

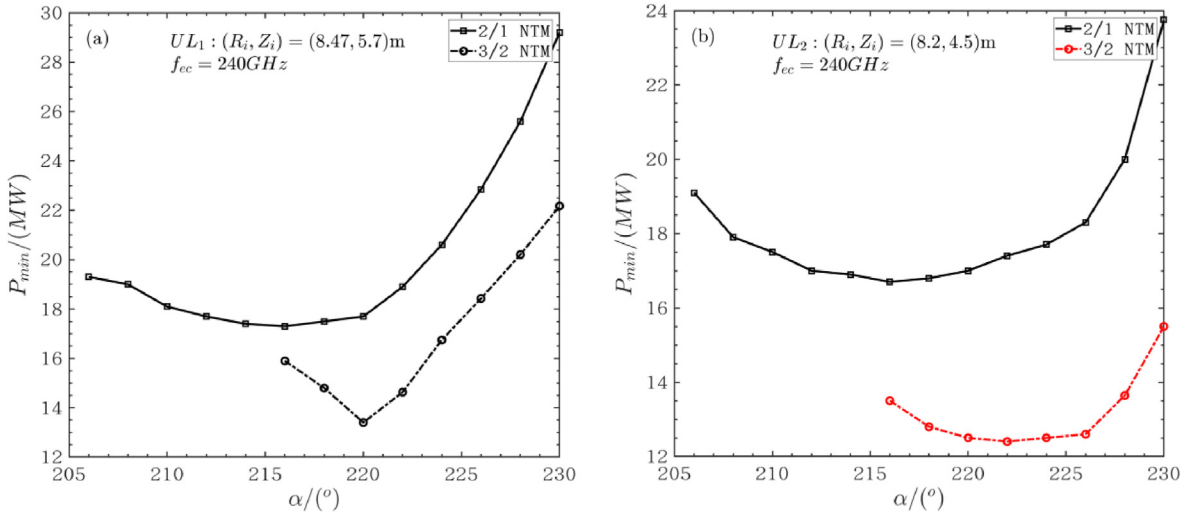

Fig. 8. The dependence of minimum EC power P_{min} on toroidal injection angle α for cases C and D. (a) Results of case C. (b) Results of case D. EC frequency $f_{ec} = 240$ GHz.

Table 3
The optimum results of 3/2 and 2/1 NTMs suppressing by ECCD and the injection angles of EC waves to obtain these results.

f_{ec}/(GHz)	UL	$P_{opt}(3,2)$/(MW)	$P_{opt}(2,1)$/(MW)	$(\alpha, \beta)_{3/2}$	$(\alpha, \beta)_{2/1}$
210	UL_1	25.8	26.0	(204°,150.0°)	(208°,145.0°)
	UL_2	17.9	20.6	(214°,143.1°)	(218°,137.3°)
240	UL_1	13.4	17.3	(220°,143.0°)	(216°,139.2°)
	UL_2	12.4	16.7	(220°,136.6°)	(216°,130.4°)

Table 4
The value of η_{NTM} and $(I_{tot}/I_p) \times 100\%$ under the optimum conditions presented in Table 3.

f_{ec}/(GHz)	UL	(3, 2) NTM		(2, 1) NTM	
		η_{NTM}	$(I_{tot}/I_p) \times 100\%$	η_{NTM}	$(I_{tot}/I_p) \times 100\%$
210	UL_1	0.6607	2.34%	0.6048	2.38%
	UL_2	0.6669	2.18%	0.7002	2.36%
240	UL_1	0.7027	2.20%	0.6954	2.34%
	UL_2	0.7889	2.12%	0.9707	2.25%

and EC wave frequency are also important factors. In this section, considering the UL position and EC frequency, the effect of misalignment on the 2/1 and 3/2 NTMs stabilization is analyzed.

In GRE, equation (4), equations (A.7) and (A.13) are used to evaluate the effect of misalignment on the stabilization. If the misalignment x_{dep} defined in Appendix A is large enough, which means that ECCD deposition locates near or on the X-point of a NTM magnetic island, the values of $G_{CD}(w^*, x_{dep})$ [27,40] in equation (A.7) and the function F(x) in equation (A.13) will become zero or even negative. In this cases, the ECCD has no effect on stabilizing the growth of a NTM magnetic island, and even promotes its growth.

Table 5 in Appendix B shows the results of the misalignment of ECCD on NTMs suppression. When the value of misalignment $\Delta\rho = |\rho_{ec} - \rho_{m/n}|$ does not exceed 0.015, the value of P_{min} does not increase significantly, or even decreases slightly in some cases. However, when the value of $\Delta\rho$ exceeds 0.015, the value of P_{min} increases rapidly with the increase of $\Delta\rho$. For low ECCD frequency case ($f_{ec} = 210$ GHz) launching from UL_1, the value of P_{min} of 2/1 mode increases moderately from 26.0 MW to 34.0 MW when the

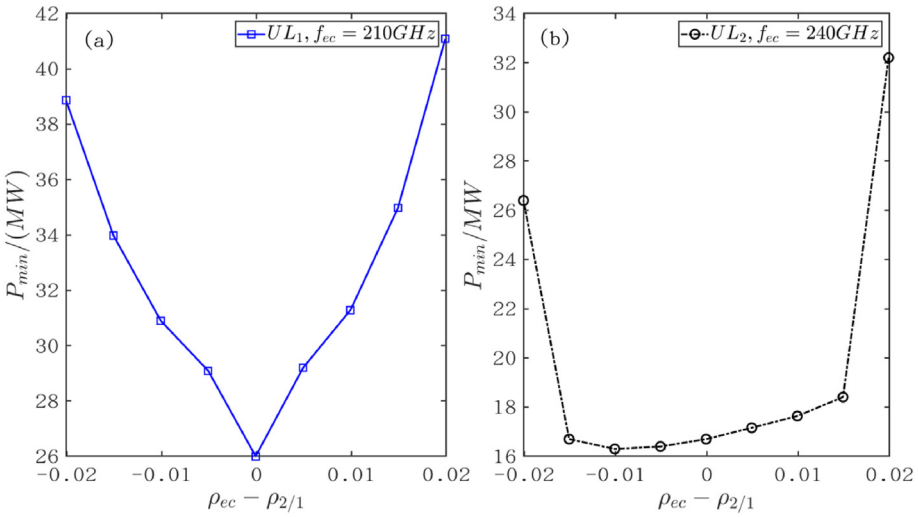

Fig. 9. The effect of the value of $\rho_{2/1}$ - ρ_{ec} on the minimum ECCD power for fully stabilizing 2/1 NTM.

misalignment $\Delta\rho$ changing from nearly zero to 0.015, then it increases to 38.9 MW when $\Delta\rho = 0.0201$. And if the value of $\Delta\rho$ increases to 0.03, after calculation, $P_{\min}$ increases to 58.7 MW which is twice more than that 26.0 MW.

It is worth noting that when the misalignment value does not exceed 0.015, the value of $P_{\min}$ changes slowly with the increase of $\Delta\rho$ in most cases, and even decreases slightly. This is mainly due to the reduction of the radial position, the value of ρ_{ec} of the ECCD, which reduces the electron trapping effect [41,42], and thus increases the current drive efficiency of the ECCD. This can be seen from table 5 that the value of j_{ec} increase with the decrease of ρ_{ec}. It can be predicted that when the value of misalignment $\Delta\rho$ is caused by the increase of ρ_{ec}, then the value of j_{ec} will decrease, the value of $P_{\min}$ will not change slightly with the increase of ρ_{ec}, but will increase more with the increase of ρ_{ec}. It is precisely because the current drive of ECCD on both sides of the rational surface of a NTM is asymmetric, resulting in asymmetric of $P_{\min}$ over misalignment $\Delta\rho$ in both side of the rational surface. A specific example of this is shown in Fig. 9, compared with the ECCD deposited on the outside of the rational surface, the misalignment of ECCD deposited on the inside of the rational surface (ρ_{ec} - $\rho_{2/1} < 0$) is better for stabilization of a NTM. The increase of the driven current of ECCD offsets the increase of $P_{\min}$ due to misalignment in this case. Therefore, the results suggest that on the CFETR tokamak, the misalignment between ECCD and NTM, $\Delta\rho$, should not exceed 0.02, preferably 0.015, and the position of ECCD should be smaller than the radial position of the rational surface of a NTM. Taking the minor radials of the CFETR, $a = 2.2$ m, it requires that the value of misalignment does not exceed 0.02×220 m $= 4.4$ cm, preferably 0.015×220 m $= 3.3$ cm.

Under the same value of misalignment $\Delta\rho$, as shown in table 5, the initial launching position and frequency of EC wave will also affect $P_{\min}$. Compared with UL_1, UL_2 is better. The higher the frequency of ECCD is, the smaller the value of $P_{\min}$ is, and as shown in Fig. 9 the sensitivity of $P_{\min}$ to misalignment $\Delta\rho$ is smaller within the range of $\Delta\rho \leq 0.015a$. When the value of misalignment $\Delta\rho$ does not exceed $0.015a$, it can be obtained from table 5 that the total ECCD current ($I_{tot} = I_{ec} \cdot P_{\min}$) required to completely suppress these NTMs does not exceed 3.2% of the plasma current I_p.

Some effects of misalignment are discussed in this section, but as the misalignment changes in time due to equilibrium evolution, a more accurate method is to use integrated modelling to assess the impact of this effect [14–17]. However, the impact of this effect should be included in the results of this paper, because the current generated by ECCD injection is still small, as shown in Table 4, which is far less than the total plasma current, $(I_{tot}/I_p) \times 100\% < 2.5\%$, hence the misalignment changes due to this effect should be small. In addition, although the misalignment discussed in this paper is achieved by changing the injection angle of the EC wave, it should be understood that this misalignment is caused by various effects, such as the equilibrium evolution over time.

4. Summary and conclusion

Just as ECCD is important for the ITER operation [40], the China Fusion Engineering Test Reactor (CFETR, $R = 7.2$ m, $a = 2.2$ m, $B_T = 6.5$ T) operation also requires ECCD to drive local current to achieve various goals, one of which is that ECCD suppresses NTMs, especially the 3/2 and 2/1 NTMs. In this paper, the minimum EC power required for complete suppression of the 3/2 and 2/1 NTMs in the CFETR hybrid operation scenario is studied by coupling the ray-tracing code for computing ECCD with the modified Rutherford equation (MRE). Although the selection of the frequency of the final EC system of the CFETR device and the position of the launching port has not been completely determined, according to the results of literature researches [4,6,7], this paper selects two typical frequencies, $f_{ec} = 210$ GHz [6] and 240 GHz [4,7] with fundamental ordinary mode launching from two different upper launcher ports, UL_1: $(R_i, Z_i) = (8.47, 5.7)$ m [6] and UL_2: $(R_i, Z_i) = (8.20, 4.5)$ m [4,7], and calculates the minimum ECCD power $P_{\min}$ to completely suppress these NTMs. The effects of the incident angles (especially the toroidal incident angle α) and the misalignment on NTMs suppression are studied and discussed in detail.

Under the condition of precise alignment, the optimal results of complete suppression of the 3/2 and 2/1 NTMs by ECCD with the two different frequencies launching from the UL_1 and UL_2 ports are listed in Table 3. The results show that the UL_2 launcher port is better than UL_1, and the optimal minimum ECCD power obtained by optimizing the incidental angles at higher frequencies is smaller. For the 2/1 NTM located at $\rho_{2/1} = 0.5576$, the optimal value of $P_{\min}$ is 20.6 MW by ECCD with $f_{ec} = 210$ GHz launching from UL_2, and a smaller $P_{\min} = 16.7$ MW by ECCD with $f_{ec} = 240$ GHz launching from the same port. For the 3/2 NTM located at $\rho_{3/2} = 0.4321$, the corresponding optimal values of $P_{\min}$ are 17.9 MW and 12.4 MW with the ECCD of the two frequencies launching from the UL_2.

The misalignment $\Delta\rho = |\rho_{ec} - \rho_{m/n}|$ between the ECCD and m/n rational surface has an important influence on NTM suppression. According to the researches in this paper, the results suggest that on the CFETR tokamak, the misalignment $\Delta\rho$ should not exceed $0.02a$,

preferably 0.015a, corresponding to 4.4 cm and 3.3 cm respectively. Within this range, the required ECCD power does not increase significantly. When good alignment cannot be achieved, the position of ECCD should be smaller than the radial position of the rational surface of a NTM due to enhancement of ECCD current drive efficiency.

If do not consider the engineering difficulty of high-frequency gyrotron source, ECCD with fundamental ordinary mode of frequency 240 GHz launching from the UL_2 port can most effectively suppress the 3/2 and 2/1 NTMs under the four cases set in this paper, and the optimal value of P_{min} in these cases is minimum, 12.4 MW and 16.7 MW respectively. However, this EC source selection is difficult to achieve in the short or medium term, lower frequency of 210 GHz may be easier to obtain. The optimal minimum EC power for the 3/2 and 2/1 NTM suppression when launching from UL_2 port is 17.9 MW and 20.6 MW using 210 GHz source, respectively. This power demand is acceptable. When pre-emptive ECCD technology [43,44] is used for NTM control, the required EC power will be greatly reduced, the saved EC power can be used for other heating and current drive requirements on the CFETR to improve the fusion gain. In view of this, it is a good choice to select 210 GHz EC wave and launching from the UL_2 port in the short and medium term. Since this article does not consider the evolution of the magnetic equilibrium configuration over time after ECCD injection, the integrated modelling to evaluate the results of this paper needs to be done.

Declaration of competing interest

The authors declare that they have no known competing financial interests or personal relationships that could have appeared to influence the work reported in this paper.

Acknowledgement

This work is supported by the National MCF Energy R & D Program (Grant Nos. 2022YFE03070003), the National Natural Science Foundation of China (Grant Nos. 12075114), the Natural Science Foundation of Hunan Province (No. 2021JJ30569), the Excellent Youth Project of Hunan Education Department (No. 19B483), the Doctoral Initiation Fund Project of University of South China (No. 190XQD114), and the Opening Project of Nuclear Fuel Cycle Technology and Equipment, University of South China (No. 2019KFZ02, 2019KFQ12).

Appendix A

The evolution of the island width w of a NTM is govern by the MRE (4) with the contribution of external ECCD. In this appendix, each term in the right-hand-side of equation (4) is described detail. The perturbed bootstrap current drives an instability, following references [26,27],

$$r_s\Delta'_{BS}=\frac{16\mu_0 L_q r_s}{B_\theta \pi}\frac{4}{3w}f(w,W_{marg})j_{BS} \tag{A.1}$$

W_{marg} is the marginal island size at which a NTM growth rate reaches maximum. According to Ref. [45], $W_{marg}\approx 2\varepsilon^{1/2}\rho_{\theta i}$. Here, $\varepsilon = r/R$ is the local inverse aspect ratio at minor radius r for major radius on the axis R, and $\rho_{\theta i}=(2m_i k_B T_i/e^2 B_\theta^2)^{1/2}$ is local poloidal ion gyro-radius for the ion mass m_i, the Boltzman constant k_B (in units of $J\cdot keV^{-1}$), the ion temperature T_i and the poloidal magnetic field B_θ, and $L_q = q/(dq/dr)$ is the local magnetic shear length. The factor $f(w, W_{marg})$ introduced in equation (A.1) to describe the limitation of the neoclassical drive for small island sizes below W_{marg}, two choices about $f(w, W_{marg})$ can be used [46]. For the first choice, the limitation comes from the stabilizing ion polarization effect, $f_{pol}(w, W_{marg}) = 1-\frac{W_{marg}^2}{3w^2}$. In this case the marginal island size is expected to scale with the ion banana width, $W_{marg}\approx 2\varepsilon^{1/2}\rho_{\theta i}$, and this choice is referred to as the "polarization" model labeled with 'pol'. The second choice, $f_{tra}(w, W_{marg})=\frac{w^2}{w^2+W_{marg}^2}$, it describes the incomplete flattening the pressure gradient inside the magnetic island as a consequence of a finite parallel transport time scale. In this case, $W_{marg}\propto(\chi_\perp/\chi_\parallel)^{1/4}$, $\chi_\perp$ and $\chi_\parallel$ are the perpendicular and parallel heat diffusivity, respectively. This choice is referred to as the "transport" model labeled with 'tra'. It is assumed here that both the "polarization" and "transport" limit the neoclassical drive with the same $W_{marg}\approx 2\varepsilon^{1/2}\rho_{\theta i}$. Hence, $f(w, W_{marg}) = f_{pol}(w, W_{marg}) + f_{tra}(w, W_{marg})$ - 1.

For the stabilization terms by current drive, there are two stabilizing effects of ECCD. For the first effect, the ECCD replaces the missing bootstrap current in the island [26,27],

$$r_s\Delta'_{CD}=-\frac{16\mu_0 L_q}{B_\theta\pi}\frac{\eta_{CD}P_{in}}{w_{dep}^2}F_{CD}\left(w\Big/w_{dep},x_{dep},D_m,\varphi_m\right) \tag{A.2}$$

F_{CD} is effectiveness parameter for replacing the missing bootstrap current, it depends on the ratio of the island width w over the full Gaussion width w_{dep} of the ECCD profile w_{dep}, i.e. $w^* = w/w_{dep}$, the misalignment with respect to the rational surface $x_{dep} = r_{dep}$ - r_{rs}, the duty cycle D_{mod} and phase φ_{mod} of EC power modulation. Where, $r_{dep} = \rho_{ec}\cdot a$ and $r_{rs} = \rho_{m/n}\cdot a$. P_{in} is the total injected EC power, and $\eta_{CD}\equiv I_{tot}/P_{in}$, I_{tot} is the total driven current by EC waves.

Assuming an identical Gaussion profile for the driven current density $\propto exp[-4(x-x_{dep})^2/w_{dep}^2]$, the total driven current [26] is

$$I_{tot}=\sqrt{k}\pi^{3/2}r_s w_{dep} \tag{A.3}$$

for an elongated plasma, where $\sqrt{k}$ is a fitting parameter which makes the I_{tot} approximately equal to the total driven current by ray-tracing code. The value of k approximately equals to the elongation of tokamak if the driven current density profile nears a Gaussion. Then, equation (A.2) becomes

$$r_s\Delta'_{CD}=-\frac{16\mu_0 L_q r_s}{B_\theta\pi}\frac{\pi^{3/2}\sqrt{k}j_{CD,max}}{w_{dep}}F_{CD} \tag{A.4}$$

Following the work of De Lazzari et al. [27], under the following two assumptions: firstly the effect of relative misalignment with respect to the rational surface to depend weakly on w*; and secondly the dependence on the on-time fraction, within a good approximation (~10%), not to change for different values of x_{dep}. Then, time consuming numerical calculation for the F_{CD} in equation (A.2) can be factorized into three figures of merit to achieve a fast calculation of the MRE,

$$F_{CD}=N_{CD}(w^*)G_{CD}\left(w^*,x_{dep}\right)M_{CD}(w^*,D_m) \tag{A.5}$$

with $N_{CD}(w^*)$ describes the normalization to the geometrical function depending on w^*,

$$N_{CD}(w^*)=\frac{0.25+0.24w^*}{1+0.64w^{*3}+0.43w^{*2}+1.5w^*} \tag{A.6}$$

$G_{CD}(w^*, x_{dep})$ accounts for the misalignment [27,40],

$$G_{CD}\left(w^*, x_{dep}\right) = 1 - 2\frac{x_{dep}}{g(w^*)} e^{-\left(\frac{x_{dep}}{g(w^*)}\right)^2} \int_0^{x_{dep}/g(w^*)} dt e^{t^2} \quad (A.7)$$

with

$$g(w^*) = \frac{0.38w^{*2} + 0.26w^* + 0.5}{w^* + 1} \quad (A.8)$$

and $M_{CD}(w^*, D_m)$ for the modulation,

$$M_{CD}(w^*, D_m) = \frac{1}{w^{*3}}\left[m_1(D_m)w^{*2} + m_2(D_m)\right] + m_3(D_m) \quad (A.9)$$

where,

$$m_1 = 2.26D_m^4 - 3.44D_m^3 - 0.99D_m^2 + 2.2D_m - 0.02 \quad (A.10)$$

$$m_2 = 0.01\left(0.34D_m^5 - 1.02D_m^4 + 0.87D_m^3 - 0.28D_m^2 + 0.1D_m\right) \quad (A.11)$$

$$m_3 = 1.34D_m^4 - 3.54D_m^3 + 1.1D_m^2 + 2.09D_m + 0.01 \quad (A.12)$$

The M_{CD} accounts for the effect of modulation as a function of the on-time fraction D_m assuming perfect phasing of the modulation centered around the island O-point. M_{CD} is optimum for modulating EC power with 40%–60% on-time fraction, in this paper only the 50% on-time fraction modulation is considered, hence $D_m = 0.5$.

The second stabilizing effect of ECCD is to make $r_s\Delta_0'$ more negative, it depends on the relative magnitude of the ECCD, $j_{CD,max}$. According to the analytical models in Refs. [26,45,47],

$$r_s\delta\Delta_0' \approx -\frac{4\mu_0 L_q r_s}{B_\theta \pi}\frac{\pi^{3/2}\sqrt{k} j_{CD,max} D_m}{w_{dep}} erfc(w^*)F(x) \quad (A.13)$$

$erfc(x) = \frac{2}{\sqrt{\pi}}\int_x^\infty e^{-t^2}dt = 1 - erf\,(x)$ is the complementary error function. And

$$F(x) = 1 - 2.92x + 2.02x^2 - 0.40x^3, \quad (A.14)$$

with $x = x_{dep}/w_{dep}$. The function (A.14) differs from $F(x)$ in Ref. [45] is that the $1/e$ full width of driven current profile w_{dep} is used in this paper, whereas full width at half maximum (FWHM) value of ECCD profile δ_{ec} is used in Ref. [45], so that $\delta_{ec} = \sqrt{ln\,2}w_{dep}$.

For the linear stability index Δ_0', a value of $r_s\Delta_0' = -m$ for the m/n mode is used in equation (4) according to Refs. [45,48]. The value, as a 'middle' one, is between strong stability, $r_s\Delta_0' \approx -2m$, and marginal classical stability, $r_s\Delta_0' = 0$.

Appendix B

Table 5
Results of the misalignment of ECCD on NTMs suppression.

f_{ec}/(GHz)	UL	(m, n) mode	α/(°)	β/(°)	j_{ec}/(A/cm^2/MW)	ρ_{ec}	w_{dep}/a	I_{ec}/(kA/MW)	P_{min}/(MW)	$\Delta\rho$=$\lvert\rho_{ec}$-$\rho_{m/n}\rvert$
210	UL_1	(2, 1)	208	145.0	0.4050	0.5575	0.1090	11.90	26.0	0.0001
				145.2	0.4068	0.5525	0.1100	11.95	29.1	0.0051
				145.4	0.4087	0.5475	0.1113	12.00	30.9	0.0101
				144.6	0.4107	0.5425	0.1115	12.05	34.0	0.0151
				145.7	0.4125	0.5375	0.1120	12.07	38.9	0.0201
		(3, 2)	204	150.0	0.5041	0.4325	0.1070	11.81	25.8	0.0004
				150.2	0.5229	0.4275	0.1042	11.85	25.5	0.0046
				150.4	0.5398	0.4225	0.1018	11.88	26.4	0.0096
				150.6	0.5586	0.4175	0.0994	11.92	28.7	0.0146
				150.8	0.5822	0.4125	0.0956	11.95	34.5	0.0196
	UL_2	(2, 1)	218	137.3	0.5918	0.5575	0.0915	14.89	20.6	0.0001
				137.5	0.596	0.5525	0.0918	14.97	20.5	0.0051
				137.7	0.5994	0.5475	0.0850	15.04	22.1	0.0101
				138.1	0.6072	0.5425	0.0932	15.19	23.9	0.0151
				138.3	0.6116	0.5375	0.0936	15.26	28.9	0.0201
		(3, 2)	214	143.1	0.7261	0.4325	0.1018	15.86	17.9	0.0004
				143.3	0.7278	0.4275	0.1028	15.91	18.4	0.0046
				143.5	0.7303	0.4225	0.1040	15.95	19.5	0.0096
				143.7	0.7337	0.4175	0.1048	16.00	21.5	0.0146
				143.9	0.7385	0.4125	0.1056	16.04	25.0	0.0196
240	UL_1	(2, 1)	216	139.2	0.6998	0.5575	0.0927	17.57	17.3	0.0001
				139.4	0.7053	0.5525	0.0930	17.68	17.2	0.0051
				139.8	0.7229	0.5475	0.0932	17.90	17.4	0.0101
				140.0	0.7303	0.5425	0.0934	18.01	19.8	0.0151
				140.2	0.7363	0.5375	0.0936	18.11	24.0	0.0201
		(3, 2)	220	143.0	1.0220	0.4325	0.0950	21.33	13.4	0.0004
				143.4	1.1064	0.4275	0.0884	21.42	13.1	0.0046
				143.8	1.2032	0.4225	0.0826	21.46	13.0	0.0096
				144.2	1.3149	0.4175	0.0758	21.44	13.4	0.0146
				144.4	1.3613	0.4125	0.0734	21.42	18.4	0.0196
	UL_2	(2, 1)	216	130.4	1.0120	0.5575	0.0633	17.49	16.7	0.0001
				131.0	1.0368	0.5525	0.0635	17.75	16.4	0.0051
				131.4	1.0481	0.5475	0.0640	17.92	16.3	0.0101
				131.6	1.0502	0.5425	0.0643	18.01	16.7	0.0151
				132.0	1.0635	0.5375	0.0647	18.18	26.4	0.0201
		(3, 2)	222	136.6	1.2400	0.4325	0.0822	22.18	12.4	0.0004
				137.0	1.2742	0.4275	0.0818	22.36	12.2	0.0046
				137.2	1.2901	0.4225	0.0818	22.45	12.2	0.0096
				137.6	1.3370	0.4175	0.0806	22.60	12.8	0.0146
				137.8	1.3623	0.4125	0.0800	22.66	16.6	0.0196

References

[1] Yuanxi Wan, Jiangang Li, Yong Liu, Xiaolin Wang, Vincent Chan, Changan Chen, Xuru Duan, Peng Fu, Xiang Gao, Kaiming Feng, Overview of the present progress and activities on the CFETR, Nucl. Fusion 57 (2017), 102009.

[2] G. Zhuang, G.Q. Li, J. Li, Y.X. Wan, Y. Liu, X.L. Wang, Y.T. Song, V. Chan, Q.W. Yang, B.N. Wan, X.R. Duan, P. Fu, B.J. Xiao, The CFETR design team, progress of the CFETR design, Nucl. Fusion 59 (2019), 112010.

[3] Jinxing Zheng, Jinggang Qin, Kun Lu, Min Xu, Xuru Duan, Guosheng Xu, Jiansheng Hu, Xianzu Gong, Qing Zang, Zhihong Liu, Liang Wang, Rui Ding, Jiming Chen, Pengyuan Li, Lei Xue, Lijun Cai, Yuntao Song, Recent progress in Chinese fusion research based on superconducting tokamak configuration, Innovation 3 (2022), 100269.

[4] J.L. Chen, V.C. Chan, X. Jian, X.J. Zhang, Q.R. Ren, G.Q. Li, C.X. Zhou, CFETR Physics Team, Integrated modeling of CFETR hybrid scenario plasmas, Nucl. Fusion 61 (2021), 046002.

[5] M. Henderson, G. Saibene, C. Darbos, D. Farina, L. Figini, M. Gagliardi, F. Gandini, T. Gassmann, G. Hanson, A. Loarte, T. Omori, E. Poli, D. Purohit, K. Takahashi, The targeted heating and current drive applications for the ITER electron cyclotron system, Phys. Plasmas 22 (2015), 021808.

[6] W.E.I. Wei, Xiaojie Wang, L.I. Miaohui, D.I.N.G. Bojiang, Evaluation of electron cyclotron current drive performance for CFETR, Plasma Sci. Technol. 21 (2019), 065101.

[7] L.H. He, P.W. Zheng, Z.H. Wang, J.L. Chen, T. Yu, Numerical investigation of ECCD under the CFETR concept design parameters, Fusion Eng. Des. 182 (2022), 113236.

[8] E. Poli, G. Tardini, H. Zohm, E. Fable, D. Farina, L. Figini, N.B. Marushchenko, L. Porte, Electron-cyclotron-current-drive efficiency in DEMO plasmas, Nucl. Fusion 53 (2013), 013011.

[9] R.J. La Haye, Neoclassical tearing modes and their control, Phys. Plasmas 13 (2006), 055501.

[10] C.C. Hegna, J.D. Callen, On the stabilization of neoclassical magnetohydrodynamic tearing modes using localized current drive or heating, Phys. Plasmas 4 (1997) 2940.

[11] H. Zohm, G. Gantenbein, F. Leuterer, M. Maraschek, E. Poli, L. Urso, Control of NTMs by ECCD on ASDEX Upgrade in view of ITER application, Plasma Phys. Contr. Fusion 49 (2007) B341.

[12] Jing-Chun Li, Xue-Yu Gong, Jia-Qi Dong, Jun Wang, Lan Yin, Numerical analysis of the optimized performance of the electron cyclotron wave system in a HL-2M tokamak, Chin. Phys. B 25 (2016), 045201.

[13] A.A. Molavi-Choobini, A. Naghidokht, Z. Karami, Study of lower hybrid current drive for the demonstration reactor, Nucl. Eng. Technol. 48 (2016) 711–718.

[14] Kyungjin Kim, Na Yong-Su, Minhwa Kim, Y.M. Jeon, K.D. Lee, J.G. Bak, M.J. Choi, G.S. Yun, S.G. Lee, S. Park, J.H. Jeong, L. Terzolo, D.H. Na, M.G. Yoo, KSTAR Team, Experiment and simulation of tearing mode evolution with electron cyclotron current drive in KSTAR, Curr. Appl. Phys. 15 (2015) 547–554.

[15] Kyungjin Kim, Na Yong-Su, Hyun-Seok Kim, M. Maraschek, E. Poli, J. Stober, H. Zohm, F. Felici, O. Sauter, Y.S. Park, L. Terzolo, ASDEX Upgrade team, TCV Team, Modeling of neoclassical tearing mode stabilization by electron cyclotron heating and current drive in tokamak plasmas, Curr. Appl. Phys. 16 (2016) 867–875.

[16] M. Kim, Kyungjin Kim, M.G. Yoo, D.H. Na, T.S. Hahm, Y.S. Hwang, Na Yong-Su, Numerical study on neoclassical tearing mode stabilization via minimum seeking method for the island width growth rate, Nucl. Fusion 55 (2015), 023006.

[17] M. Kim, Na Yong-Su, Kyungjin Kim, H.-S. Kim, D.H. Na, M.G. Yoo, T.S. Hahm, Y.S. Hwang, Reply to 'Comment on "Numerical study on neoclassical tearing mode stabilization via minimum seeking method for the island width growth rate", Nucl. Fusion 56 (2016), 038002.

[18] N. Bertelli, G. Wallace, P.T. Bonoli, R.W. Harvey, A.P. Smirnov, S.G. Baek, R.R. Parker, C.K. Phillips, E.J. Valeo, J.R. Wilson, J.C. Wright, The effects of the scattering by edge plasma density fluctuations on lower hybrid wave propagation, Plasma Phys. Contr. Fusion 55 (2009), 074003.

[19] E. Mazzucato, I. Fidone, G. Granata, Damping of electron cyclotron waves in dense plasmas of a compact ignition tokamak, Phys. Fluids 30 (1987) 3745.

[20] Y.R. Lin-Liu, V.S. Chan, R. Prater, Electron cyclotron current drive efficiency in general tokamak geometry, Phys. Plasmas 10 (2003) 4064.

[21] N.B. Marushchenko, H. Maassberg, Yu Turkin, Electron cyclotron current drive calculated for ITER conditions using different models, Nucl. Fusion 48 (2008), 054002.

[22] N.B. Marushchenko, H. Maassberg, Yu Turkin, Corrections to the paper 'electron cyclotron current drive calculated for ITER conditions using different models, Nucl. Fusion 49 (2009), 129801.

[23] Jingchun Li, Chijie Xiao, Zhihong Lin, Dongjian Liu, Xiaoquan Ji, Xiaogang Wang, GTC simulation of linear stability of tearing mode and a model magnetic island stabilization by ECCD in toroidal plasma, Phys. Plasmas 27 (2020), 042506.

[24] R.H. Cohen, Effect of trapped electrons on current drive, Phys. Fluids 30 (1987) 2442.

[25] R. Prater, D. Farina, Yu Gribov, R.W. Harvey, A.K. Ram, Y.-R. Lin-Liu, E. Poli, A.P. Smirnov, F. Volpe, E. Westerhof, A. Zvonkov, Benchmarking of codes for electron cyclotron heating and electron cyclotron current drive under ITER conditions, Nucl. Fusion 48 (2008), 035006.

[26] N. Bertelli, D. De Lazzari1, E. Westerhof, Requirements on localized current drive for the suppression of neoclassical tearing modes, Nucl. Fusion 51 (2011), 103007.

[27] D. De Lazzari, E. Westerhof, On the merits of heating and current drive for tearing mode stabilization, Nucl. Fusion 49 (2009), 075002.

[28] R.W. Harvey, M.G. McCoy, G.D. Kerbel, Power dependence of electron-cyclotron current drive for low and high-field absorption in tokamaks, Phys. Rev. Lett. 62 (1989) 426.

[29] T. Liu, Z.X. Wang, L. Wei, J.L. Wang, Prevention of electron cyclotron current drive triggering explosive bursts in reversed magnetic shear tokamak plasmas for disruption avoidance, Nucl. Fusion 62 (2022), 056018.

[30] W.K. Tang, Z.X. Wang, L. Wei, J.L. Wang, S.S. Lu, Control of neoclassical tearing mode by synergetic effects of resonant magnetic perturbation and electron cyclotron current drive in reversed magnetic shear tokamak plasmas, Nucl. Fusion 60 (2020), 026015.

[31] C.C. Petty, M.E. Austin, C.T. Holcomb, R.J. Jayakumar, R.J. La Haye, T.C. Luce, M.A. Makowski, P.A. Politzer, M.R. Wade, Magnetic-flux pumping in high-performance, stationary plasmas with tearing modes, Phys. Rev. Lett. 102 (2009), 045005.

[32] S.C. Jardin, N. Ferraro, I. Krebs, Self-organized stationary states of tokamaks, Phys. Rev. Lett. 115 (2015), 215001.

[33] Minho Park, Na Yong-Su, Jaemin Seo, M. Kim, Kyungjin Kim, Effect of electron cyclotron beam width to neoclassical tearing mode stabilization by minimum seeking control in ITER, Nucl. Fusion 58 (2018), 016042.

[34] Heinz Isliker, Ioanna Chatziantonaki, Christos Tsironis, Loukas Vlahos, Electron-cyclotron wave propagation, absorption and current drive in the presence of neoclassical tearing modes, Plasma Phys. Contr. Fusion 54 (2012), 095005.

[35] O. Chella, S. Alberti, I. Furno, T. Goodman, O. Maj, G. Merlo, E. Poli, P. Ricci, F. Riva, H. Weber, the TCV Team, Millimeter-wave beam scattering and induced broadening by plasma turbulence in the TCV tokamak, Nucl. Fusion 61 (2021), 066011.

[36] A.H. Reiman, N.J. Fisch, Suppression of tearing modes by radio frequency current condensation, Phys. Rev. Lett. 121 (2018) 225001.

[37] R.J. La Haye, J.R. Ferron, D.A. Humphreys, T.C. Luce, C.C. Petty, R. Prater, E.J. Strait, A.S. Welander, Requirements for alignment of electron cyclotron current drive for neoclassical tearing mode stabilization in ITER, Nucl. Fusion 48 (2008), 054004.

[38] E. Poli, C. Angioni, F.J. Casson, D. Farina, L. Figini, T.P. Goodman, O. Maj, O. Sauter, H. Weber, H. Zohm, G. Saibene, M.A. Henderson, On recent results in the modelling of neoclassical-tearing-mode stabilization via electron cyclotron current drive and their impact on the design of the upper EC launcher for ITER, Nucl. Fusion 55 (2015), 013023.

[39] Jing-Chun Li, Jia-Qi Dong, Xiao-Quan Ji, You-Jun Hu, Neoclassical tearing mode stabilization by electron cyclotron current drive for HL-2M tokamak, Chin. Phys. B 30 (2021), 075203.

[40] F.M. Poli, E.D. Fredrickson, M.A. Henderson, S.-H. Kim, N. Bertelli, E. Poli, D. Farina, L. Figini, Electron cyclotron power management for control of neoclassical tearing modes in the ITER baseline scenario, Nucl. Fusion 58 (2018), 016007.

[41] R. Prater, R.J. La Haye, J. Lohr, T.C. Luce, C.C. Petty, J.R. Ferron, D.A. Humphreys, E.J. Strait, F.W. Perkins, R.W. Harvey, Discharge improvement through control of neoclassical tearing modes by localized ECCD in DIII-D, Nucl. Fusion 43 (2003) 1128.

[42] R. Prater, Heating and current drive by electron cyclotron waves, Phys. Plasmas 11 (2004) 2349.

[43] R.J. La Haye, D.A. Humphreys, J.R. Ferron, T.C. Luce, F.W. Perkins, C.C. Petty, R. Prater, E.J. Strait, A.S. Welander, Higher stable beta by use of pre-emptive electron cyclotron current drive on DIII-D, Nucl. Fusion 45 (2005) L37.

[44] E. Kolemen, A.S. Welander, R.J. La Haye, N.W. Eidietis, D.A. Humphreys, J. Lohr, V. Noraky, B.G. Penaflor, R. Prater, F. Turco, State-of-the-art neoclassical tearing mode control in DIII-D using real-time steerable electron cyclotron current drive launchers, Nucl. Fusion 54 (2014), 073020.

[45] R.J. La Haye, R. Prater, R.J. Buttery, N. Hayashi, A. Isayama, M.E. Maraschek, L. Urso, H. Zohm, Cross–machine benchmarking for ITER of neoclassical tearing mode stabilization by electron cyclotron current drive, Nucl. Fusion 46 (2006) 451.

[46] O. Sautor, M.A. Henderson, G. Ramponi, H. Zohm, C. Zucca, On the requirements to control neoclassical tearing modes in burning plasmas, Plasma Phys. Contr. Fusion 52 (2010), 025002.

[47] E. Westerhof, Tearing mode stabilization by local current density perturbations, Nucl. Fusion 30 (1990) 1143.

[48] O. Sauter, R.J. Buttery, R. Felton, T.C. Hender, D F Howell and contributors to the EFDA-JET Workprogramme, Marginal β-limit for neoclassical tearing modes in JET H-mode discharges, Plasma Phys. Contr. Fusion 44 (2002) 1999.